A comparative histological study of the osteoderms in the lizards *Heloderma suspectum* (Squamata: Helodermatidae) and *Varanus komodoensis* (Squamata: Varanidae)

Alexander Kirby[1], Matt Vickaryous[2], Alan Boyde[3], Alessandro Olivo[1], Mehran Moazen[4], Sergio Bertazzo[1], Susan Evans[5]*

[1]Department of Medical Physics & Biomedical Engineering, University College London, London WC1E 6BT, UK

[2]Department of Biomedical Sciences, University of Guelph 50 Stone Road East, Guelph, ON, N1G 2W1, CANADA

[3]Dental Physical Sciences, Barts and The London School of Medicine and Dentistry, Queen Mary University of London, Mile End campus, London E1 4NS, UK

[4]Department of Mechanical Engineering, University College London, London WC1E 6BT, UK

[5]Department of Cell & Developmental Biology, University College London, London WC1E 6BT, UK

Running title: Osteoderm histology

*To whom correspondence should be addressed. Email: *s.e.evans@ucl.ac.uk*

Abstract

We describe the histological appearance of the osteoderms (ODs) of *Heloderma suspectum* and *Varanus komodoensis* using multiple staining and microscopy techniques to yield information about their morphology and development. Histological analysis showed that the ODs of *H. suspectum* are composed of three main tissue types, a superficial layer herein identified as osteodermine, capping a base composed of Sharpey-fibre bone and lamellar bone rich in secondary osteons (Haversian bone tissue). In contrast, ODs in *V. komodoensis* are composed of a core of woven bone surrounded by parallel-fibred bone without a capping tissue. Thus, between these two species, ODs differ both in terms of their structural composition and in details of their skeletogenesis. The histology of the mineralised tissues observed in these two reptile taxa provides insights into the mechanism of formation of lizard ODs and presents a direct comparison of the histological properties between the ODs of the two species. These data allow for greater understanding of the comparative histological appearance of the dermal bones of lizards and highlights their structural diversity.

Key words

"osteoderms", "histology", "polarised light", "lizard", "osteodermine", "Gila monster", "Komodo dragon"

Introduction

Osteoderms (ODs), which literally means "bone in the skin", are hard tissue organs embedded into the dermis of vertebrates (Moss, 1972), forming part of the dermal (integumentary) skeleton of tetrapods (Vickaryous & Sire, 2009). They are often referred to as "ossicles", "bony plates" or "dermal armour" among other synonyms. The histological organisation of skeletally mature ODs provides information about their mode of development (Moss, 1972; de Buffrénil et al., 2010; de Buffrénil et al., 2011), evolutionary origin and homology across species (de Buffrénil et al., 2010). Previous work has shown that OD development is not homogenous across vertebrates (Vickaryous & Sire, 2009); the mode of development of some ODs in mammals, e.g. in *Dasypus novemcinctus* Linnaeus 1758*,* the nine-banded armadillo, is comparable with intramembranously derived elements of the human skull (Vickaryous & Sire, 2009). However, in reptiles including dinosaurs (e.g. Horner et al., 2016), alligators (Vickaryous & Hall, 2008) and lizards (Zylberberg & Castanet, 1985; Levrat-Calviac & Zylberberg, 1986; Vickaryous et al., 2015), ODs have been postulated to arise via spontaneous mineralisation that forms within pre-existing dermal collagen arrangements, much like tendon ossification (Hall, 2015).

Among living tetrapods, lizards (exclusive of snakes) include the largest number of OD-bearing taxa. In this group, ODs are considered to represent a primitive trait of the basal tetrapods, lost in some later lineages (Levrat-Calviac and Zylberberg, 1986), and related to the latent ability of the dermis to generate a mineralised tissue (Main et al., 2005). OD expression within a clade is often variable, even within a single genus (Campbell, 1982). Lizard ODs have a heterogeneous tissue composition and have been described as containing woven bone (Zylberberg and Castanet, 1985), parallel-fibred bone (Vickaryous & Hall, 2008), lamellar bone (Zylberberg & Castanet, 1985; de Buffrénil et al., 2010) and Sharpey-fibre bone (Vickaryous & Hall, 2008; Vickaryous et al., 2015). This diversity in OD composition, morphology, arrangement and distribution makes lizards an ideal group in which to examine the differences in OD histology.

A recently discovered highly-mineralised OD component, osteodermine, was first named in a fossil squamate (Glyptosaurinae) from the late Cretaceous (de Buffrénil et al., 2011). Since then, this material has been observed on the superficial surface of extant *Tarentola annularis* (Geoffroy Saint-Hilaire 1827) (Vickaryous et al., 2015) and *Tarentola mauritanica* (Linnaeus 1758) (Levrat-Calviac & Zylberberg, 1986) ODs. However, relatively little has been done to characterise osteodermine histologically, nor has there been much research as to the latent ability of squamates to mineralise dermal components (Haines and Mohuiddin, 1968). Indeed, the most recent review of tetrapod ODs (Vickaryous & Sire, 2009) highlighted the gaps in our current knowledge of the skeletogenesis and subsequent material composition of squamate ODs and called for further investigation into these. A recent study compared cell-mediated mineralisation of ODs to that of heterotopic ossification in humans (Dubansky and Dubansky, 2018), emphasising the importance of understanding the ontogeny of ODs in the context of creating models for human disease.

Varanus komodoensis Ouwens 1912 (Komodo Dragon) and *Heloderma suspectum* Cope 1869 (Gila Monster) are two relatively closely related (Varanidae and Helodermatidae respectively) anguimorph squamates known to possess ODs. These ODs are distinctive among lizards, in that they are separated from one another by soft tissue, rather than forming a dense protective sheet of overlapping 'tiles' as in most scincoid and anguid lizards. Nonetheless, there are differences in the gross morphology and arrangement of the ODs in *H. suspectum* and *V. komodoensis*. In the former, the ODs form a stud-like body covering of isolated, rounded mounds, and in the latter, slender, vermiform cylinders, as well as rosette and dendritic shaped ODs mesh into an arrangement that is more like 'chain mail' (Maisano et al., 2019). This may reflect the contrasting activity patterns of the two species; the Komodo Dragon is an active predator of large mammals, whereas the Gila Monster is sluggish and spends most of its time underground.

The ODs of *H. suspectum* have been described as being composed of a basal layer of bone, but having a capping tissue of unknown composition and origin (Moss, 1972; Vickaryous

& Sire, 2009). Our objectives were firstly to provide a detailed histological characterisation of ODs from the anguimorphs *H. suspectum and V. komodoensis* and secondly, to characterise the unknown capping tissue in *H. suspectum* to test if it is osteodermine and to determine whether it is present in the ODS of *V. komodoensis*, the histology of which is currently undescribed.

Methodology

Skin Samples:

For the purposes of this study, samples of skin measuring roughly 10cm_2, were dissected from the post-cranial dorsum of *H. suspectum* and *V. komodoensis* and frozen at -20$_o$C. The lizard samples were provided by Zoological Society of London, London Zoo Pathology Department (to author Evans).

Histology:

Dissected skin samples were defrosted and fixed in 10% neutral buffered formalin for 24 hours then placed in decalcification solution (1.9% glutaraldehyde, 0.15M EDTA, in 0.06M sodium cacodylate buffer, adj. 7.4pH) at 4$_o$C, changing to fresh solution every 7 days, for 4 weeks. Further decalcification was performed prior to embedding using a Sakura TDE™30 Electrolysis Decalcifier System (Item Code 1427) and Sakura TDE™30 Decalcifier Solution (Item Code 1428) on default settings. Samples were embedded in paraffin wax and then sectioned either coronally or parasagittally, at 5µm thickness, with a HM Microm 355S automatic rotary microtome (Thermo Fisher Scientific, Waltham, MA.). These sections were stained with Haematoxylin and Eosin (H&E; Kiernan et al., 2010), Alcian blue (Klymkowsky and Hanken, 1991), Masson's trichrome (Calvi et al., 2012) or Elastic/Verhoeff Van Gieson (E.V.G./V.V.G.; Puchtler & Waldrop, 1979) (Supplementary Table 1). The slides were scanned using a Leica SCN400 scanner to create a digital image.

Cross-Polarised Light Microscopy (CPLM):

For cross-polarised light microscopy, samples were prepared as above for histology but prior to staining procedures, the dewaxed, unstained sections collected on glass slides were stained with 0.5% aqueous toluidine blue on a heated stage for 15s and the result observed through

crossed polars on a Zeiss LSM 510 Meta Laser scanning microscope.

Multi-rotation Polarised Light Microscopy:

Multi-rotation PLM was achieved by rotating crossed-polarising filters around a stationary sample –a new approach to increase the information content in polarised light microscopy of all tissues, introduced by Boyde et al. (2019). In the present study, the overwhelming PLM signal was attributable to the positive form birefringence of collagen. By sampling at close rotation intervals of 15º, the signal due to collagen fibre orientation was constant (to within 96.7%: cos 15º = 0.9659) irrespective of its axis in the plane of section. For the present study, we used automated rotation of the polarising and analysing filters at six 15º intervals with Linearly Polarised Light (LPL) images recorded at each orientation. For reference, the objectives used were 4/0.13, 10/0.30, 20/0.50 and 40/0.75. The images were merged using ImageJ in the colour circular sequence Red, Yellow, Green, Cyan, Blue, Magenta (importantly, ensuring that the intensities generated by the intermediate Y, C, M colours match those of the three primary colours, RGB). Colour in the composite image shows the orientation within the section plane, with 4 repeat cycles in 360º. Brightness was proportional to the cosine of the strike angle with respect to section plane, being brightest in plane, and black when perpendicular to that plane, i.e., parallel to the optic axis. For this study, we used H&E and Masson's Trichrome stained sections. The prior staining makes some difference to the light absorption, but did not contribute to the output colour in the combined images.

X-ray Plate Imaging:

Dissected samples were placed onto the plate detector of a Nomad Pro 2 X-ray system and exposed to X-rays from 30cm of distance with a tube voltage of 60KV and a minimum current of 2.5mA, for a duration of 0.2 seconds. The digital file was scaled using ImageJ with a control image of a radiopaque ruler.

Results

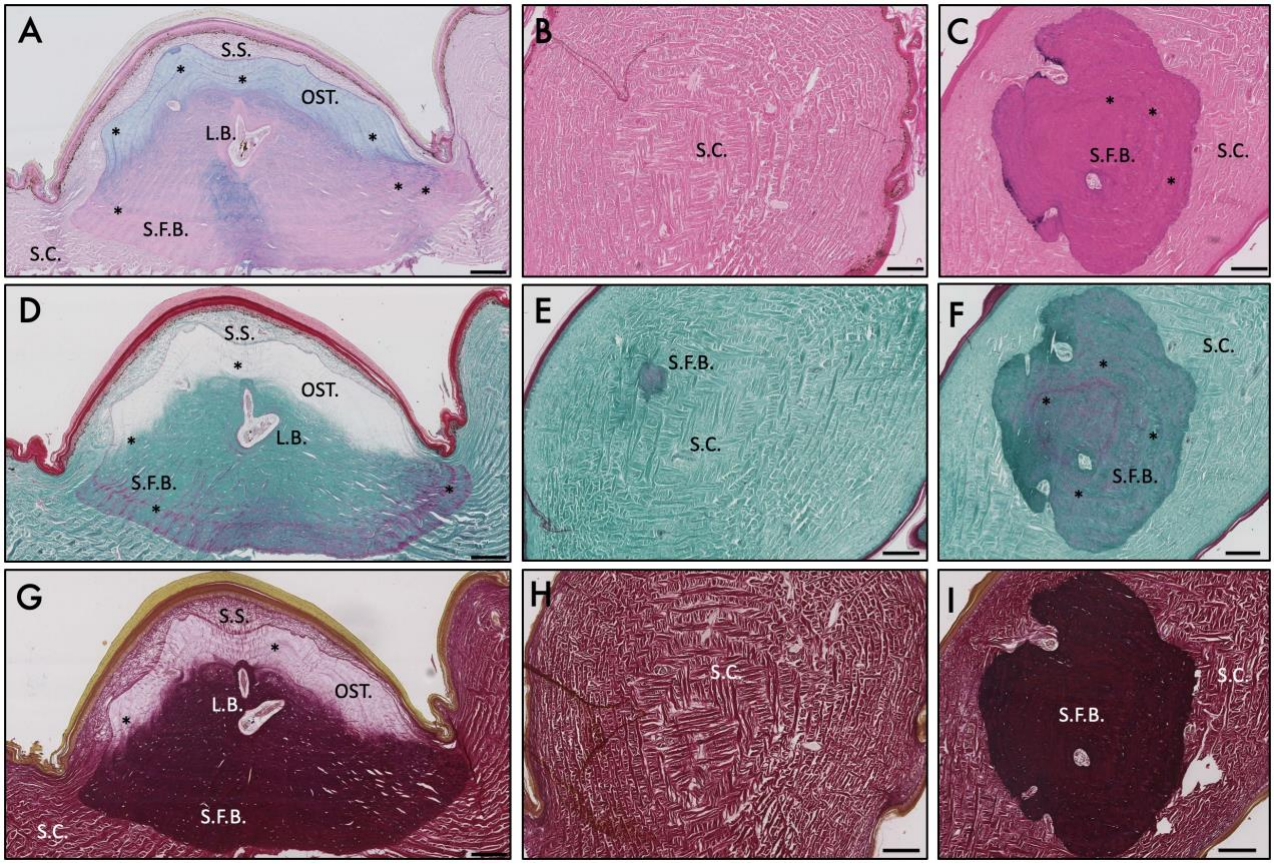

Figure 1: Histological overview of *H. suspectum* OD in (A, D, G) parasagittal and (C, F, I) coronal sections stained with (A) Alcian blue, (B, C) H&E, (D-F) Masson's trichrome and (G-I) Verhoeff van Gieson. Also (B, E, H) coronal sections of unmineralised dermis for comparison. S.F.B. = Sharpey-fibre bone, L.B. = lamellar bone, OST. = osteodermine, S.C. = stratum compactum, S.S. = stratum superficiale, Asterisks = growth lines. Scale bars: All 200µm.

Selected histological stains (Supplementary Table 1) were implemented to aid the visualisation of the structural morphology of the ODs from both species. When viewed in the dorsoventral plane using X-ray plate imaging, ODs of *H. suspectum* appeared as non-overlapping, circular shapes, roughly 2-4mm in diameter, regularly tessellated with hexagonal symmetry and displayed a rough, ornamented superficial surface (Supp. Fig. 1A). In parasagittal section (Fig. 1A), ODs of *H. suspectum* appeared lozenge-shaped with a vermiculate superficial surface, and a smooth deep surface, situated at the interface between the deep dermis (stratum compactum) and the superficial dermis (stratum superficiale) (Fig. 1B). In places, the apical surface of the OD resided in close contact (<20µm) with the stratum germinativum of the epidermis (Fig. 1A), while the basal surfaces were located at a greater distance from the

epidermis (Fig. 1C). Each OD was overlain by a single keratinised "scale" or "scute" (not to be confused with mineralised scales of fish), which stained bright red with Masson's trichrome staining (Fig. 1D, outer most layer).

In *H. suspectum,* each OD was composed of three distinct mineralised tissues: (1) osteodermine (OST.), (2) Sharpey-fibre bone (S.F.B.) and (3) lamellar bone (L.B.) The base of each OD was composed of an ossified tissue that incorporates numerous thick collagen bundles passing from the adjacent stratum compactum. Based on comparisons of similar ossified tissues rich in large collagenous fibres (e.g., Witten and Hall, 2002; Vickaryous et al., 2015), we interpret this as Sharpey-fibre bone (S.F.B.). Weak staining with Alcian blue (Fig. 1A) indicated the presence of acid mucosubstances within the S.F.B., although no evidence of cartilage was observed. Masson's trichrome staining (Fig. 1D, E, F) revealed the characteristic presence of numerous large bundles of collagen fibres with the S.F.B., some of which were under tension (i.e., stained red; as shown under experimental tension by Flint and Merrilees, 1976), while E.V.G. staining (Fig. 1G, H, I) showed that few elastic fibres were present. S.F.B. was cellular, as evidenced by various osteocytes, and showed evidence of repeating darkly stained lines, indicative of growth and/or mineralisation fronts (Fig. 1A, D, Asterisks).

Invested within the S.F.B. were deposits of concentrically organised L.B. around endosteal surfaces of the medullary cavities and neurovascular canals, creating Haversian systems or secondary osteons (Fig. 1, L.B.). Unlike S.F.B., lamellar bone (L.B.) failed to stain with Alcian blue (Fig. 1A), but did show evidence of collagen bundles in tension (with Masson's trichrome; Fig. 1C) and the presence of elastin fibres in the lumen of the canal (E.V.G. staining; Fig 1G).

Capping each *H. suspectum* OD, residing in the non-mineralised stratum superficiale, was an unusual tissue herein identified as osteodermine (Fig. 1A, D, G, OST.). Matching previous reports (de Buffrénil et al., 2011; Vickaryous et al., 2015), *H. suspectum* osteodermine is collagen-poor, essentially acellular, and demonstrates evidence of periodic growth. *H. suspectum* osteodermine stained weakly for Alcian blue (Fig. 1A), indicating the presence of acid

198 mucosubstances, lacked intrinsic collagen (as revealed by Masson's trichrome; Fig. 1D) and
199 elastin (using E.V.G.; Fig. 1G), and showed evidence of periodic growth (Fig. 1, Asterisks).
200 In contrast to the robust, bead-shaped ODs of *H. suspectum*, those of *V. komodoensis*
201 resembled smooth, slightly bent cylinders, roughly 2-4mm in length and partially overlapping
202 one another (Supp. Fig. 1B). Accordingly, the morphology of these elements has been described
203 as vermiform (e.g., Erickson et al., 2003). In addition to gross morphology, ODs in *V.*
204 *komodoensis* also differ from those of *H. suspectum* at the level of serial histology. For example,
205 in *V. komodoensis*, ODs were found invested within the deep dermis (stratum compactum) (Fig.
206 2A, SC), while those of *H. suspectum* were located at the interface between the superficial

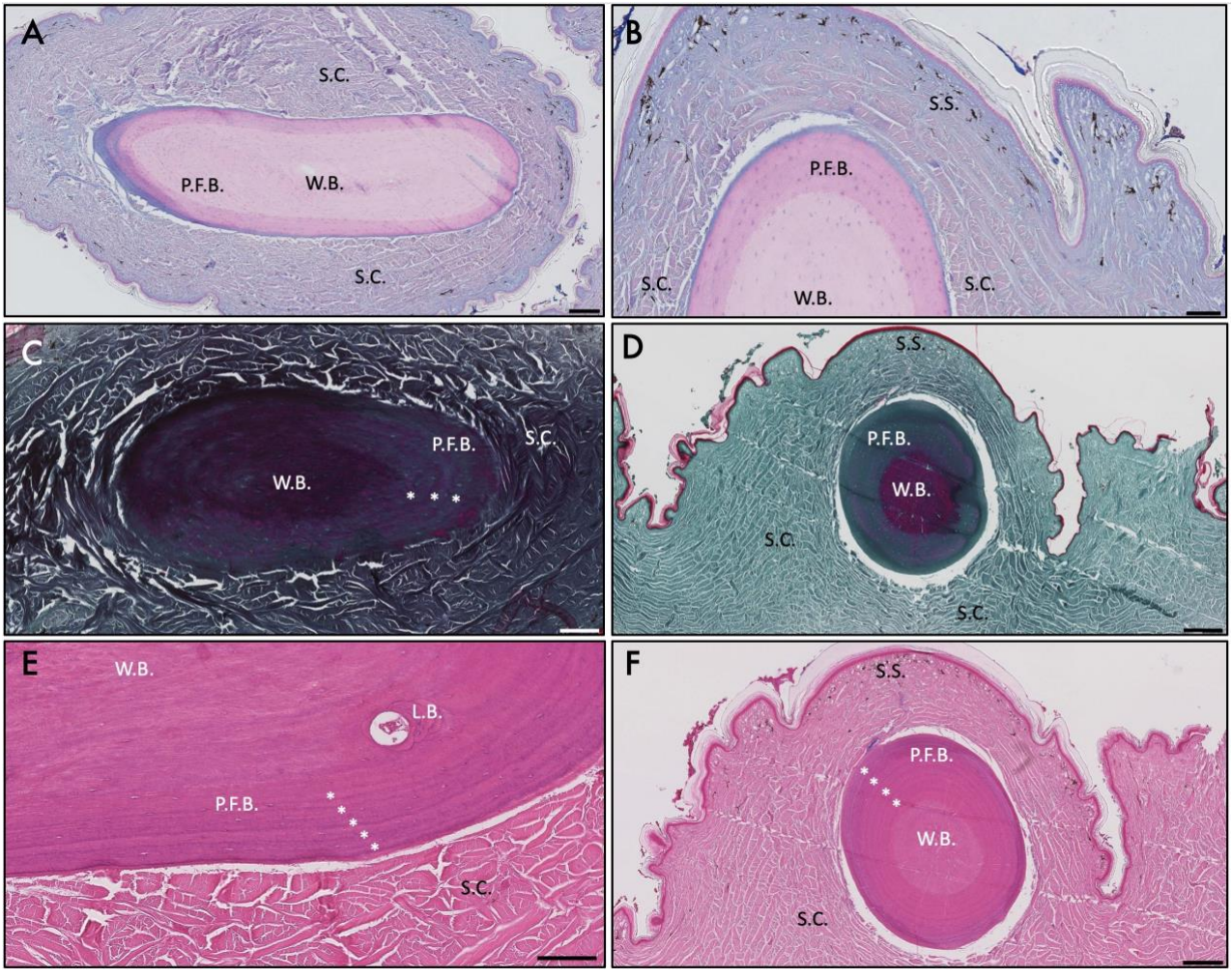

Figure 2: Histological overview of *V. komodoensis* OD stained with Alcian blue in (A) parasagittal and (B) coronal section, stained with Masson's trichrome in (C) parasagittal and (D) coronal section; and stained with Haematoxylin and Eosin in (E) parasagittal section and (F) coronal section. L.B. = lamellar bone, W.B. = woven bone, P.F.B. = parallel-fibred bone, S.C. = stratum compactum, S.S. = stratum superficiale, Asterisks = growth lines. Scale bars: (A) = 200µm, (B and C) = 100µm, (D) = 200µm, (E) = 100µm, (F) = 200µm.

(stratum superficiale) and deep dermal compartments. In addition, *V. komodoensis* ODs lacked Sharpey-fibre bone and osteodermine. Instead, they were primarily composed of: (1) woven bone (2) lamellar bone and (3) parallel-fibred bone. In section, *V. komodoensis* ODs had a conspicuous concentric arrangement of outer rings and an inner core (Fig. 2). The inner core region was composed of woven bone, exhibiting a densely packed arrangement of interlacing, randomly arranged mineralised collagen fibres. The woven bone core was negative for acid mucosubstances (Fig. 2A, B) and showed evidence of collagen fibres in tension (Fig. 2C, D). The outer rings were composed of parallel-fibred bone, with closely packed and regularly arranged collagen fibres. The periphery of each OD is surrounded by a thin layer of Alcian blue-positive osteoid (unmineralised bone; Fig. 2A, B). We also observed evidence of remodeling, with deposits of lamellar bone (L.B.) contributing the formation of an osteon (Fig 2E), as well as concentric lines of growth (Fig. 2F, Asterisks).

To further investigate the relationship between ODs and the dermis, we used polarised light microscopy (Fig. 3). In *H. suspectum* ODs, the boundary between the mineralised (S.F.B.) and the non-mineralised stratum compactum (S.C.) was almost indistinguishable, with regularly interspaced bundles of collagen fibres of the dermis passing uninterrupted into the mineralised OD (Fig. 3A). In contrast, for *V. komodoensis* ODs there was a sharp boundary between bone and dermis, with only occasional Sharpey's fibres anchoring the skeletal element into the surrounding skin (Fig. 3B white arrows). The same circumstances were observed in coronal sections of both species (Fig. 3C, D).

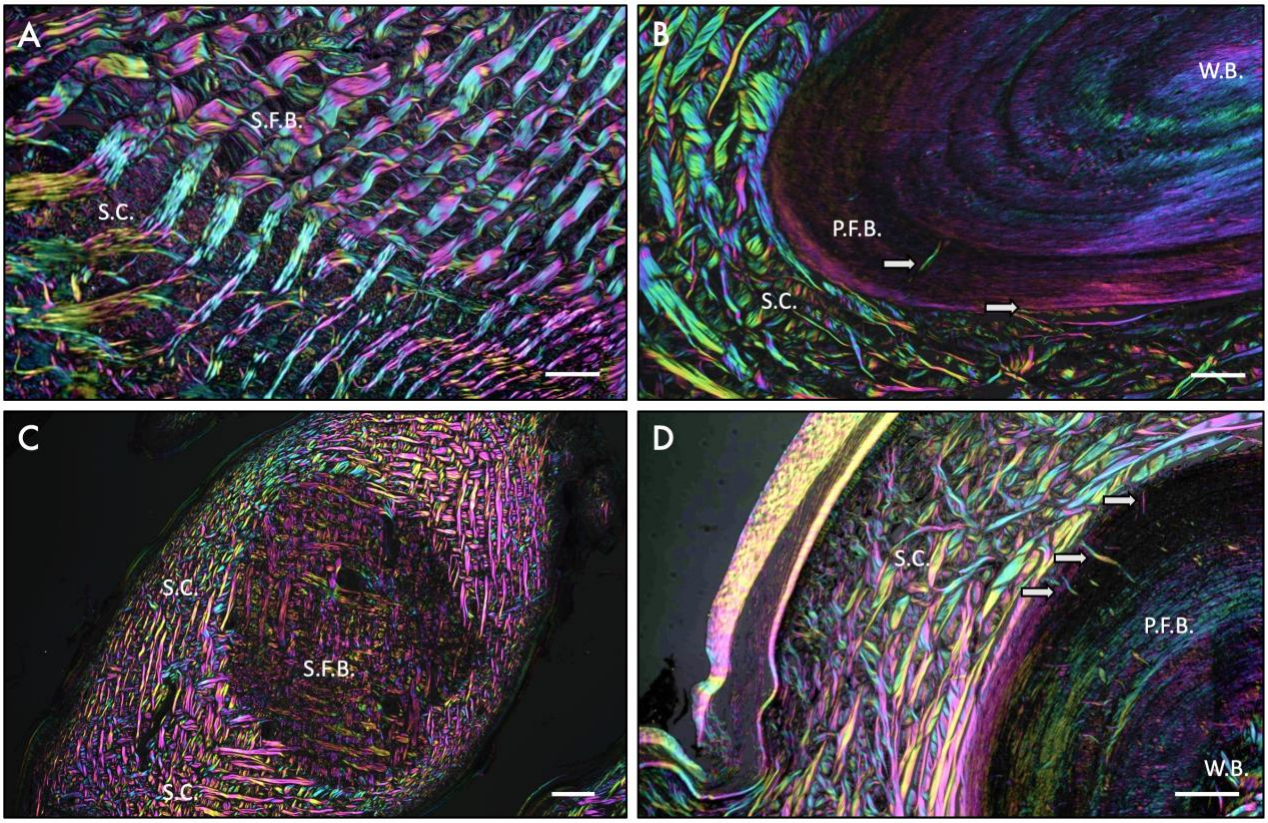

Figure 3: (A) Parasagittal section of *H. suspectum* OD, (B) parasagittal section of *V. komodoensis* OD, (C) coronal section of *H. suspectum* OD, and (D) coronal section of *V. komodoensis* OD. (A-D) All stained with H&E and visualised with multi-rotation polarised light microscopy. S.F.B. = Sharpey-fibre bone, P.F.B. = parallel-fibred bone, W.B. = woven bone, S.C. = stratum compactum, white arrows = Sharpey's fibres. Scale bars: (A) = 50µm, (B) = 50µm, (C) = 250µm, (D) = 50µm.

In *H. suspectum,* osteodermine failed to stain with toluidine blue and displayed monorefringence when viewed using polarised light, with evidence of concentrically arranged lines of arrested growth (Fig. 4A-D, OST.). As revealed by staining with Masson's trichrome, intrinsic collagen fibres appeared to be virtually absent from the osteodermine matrix, whereas penetrating Sharpey's fibres were observed passing radially through the otherwise vitreous matrix (Fig. 4C, D, white arrows). A "Maltese cross" indicative of a secondary osteon following bone remodeling (Stump, 1925), was observed in the L.B. region across multiple sections as a cross shaped, dark formation in transmitted light (Fig. 4A, B L.B., red arrows). Occasionally, we were able to identify vascular channels that were not encased by this L.B. and therefore did not produce a "Maltese cross" (Fig 4A, B). We were not able to identify a "Maltese cross" in any *V. komodoensis* sections.

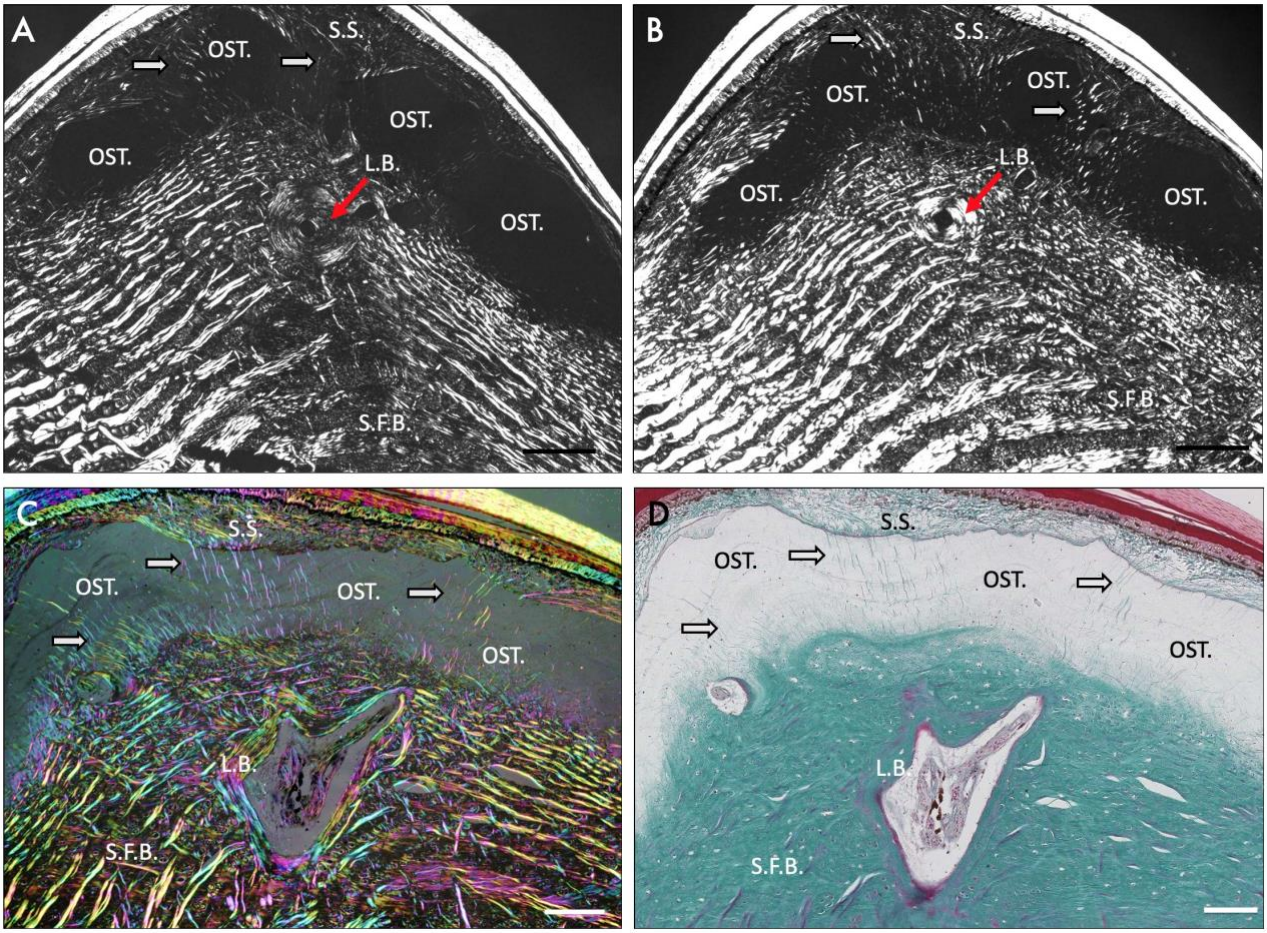

Figure 4: (A and B) Parasagittal sections of *H. suspectum* OD stained with toluidine blue visualised with cross-polarised light microscopy. (C) *H. suspectum* OD, parasagittal section stained with Masson's Trichrome, visualised with multi-rotation polarised light microscopy and (D) same section as (C), visualised with light microscopy. S.F.B. = Sharpey-fibre bone, L.B. and red arrows = lamellar bone, OST. = osteodermine, S.C. = stratum compactum, S.S. = stratum superficiale, white arrows = Sharpey's fibres. Scale bars: All 100µm.

Discussion

The primary objective of this study was to provide a detailed histological characterisation of ODs from the anguimorphs *H. suspectum* and *V. komodoensis*. The second objective was to characterise the histological appearance of osteodermine and to confirm its presence in *Heloderma suspectum* ODs.

Objective one: comparison of the OD histology between *Heloderma suspectum* and *Varanus komodoensis*

Histological results demonstrated several important differences in the staining and

248 structure of the mineralised materials present in the ODs of the two species. Whereas ODs of
249 both *H. suspectum* and *V. komodoensis* are present within the dermis and are primarily
250 composed of bone, their relative placement within the dermis and the structural organisation of
251 the ossified matrix differs notably between the two species. In addition, *H. suspectum* develops a
252 conspicuous capping tissue (herein identified as osteodermine) whereas *V. komodoensis* does
253 not. Taken together, these data suggest that disparity in OD structure reflects fundamental
254 differences in the functional role and evolutionary history of these elements. As explained in the
255 introduction, Gila monsters are understood to be lethargic hunters, whereas Komodo dragons
256 are active hunters. Therefore, it seems likely that differences in OD structural composition
257 reflect the different ecological environments of the dermis within the distinct predatorial niches
258 that these two species occupy. Accordingly, future studies are welcomed that attempt to
259 elucidate a clear correlation between ecological environment and the histology of lizard ODs.
260 Whereas the dermis represents the structural milieu of OD formation, there are
261 differences across species in the relative position of the skeletally mature elements. As is the
262 case seen in *Varanus salvator* (Erickson et al., 2003), the ODs of *V. komodoensis* were situated
263 comparatively deep within the stratum compactum of the dermis, whereas those of *H.*
264 *suspectum* were located at or near the interface between the stratum superficiale and
265 compactum. A similar position has also been described for the OD (and osteodermine)-bearing
266 geckos *T. mauritanica* and *T. annularis* (Vickaryous, et al., 2015). This raises the possibility that
267 the formation of osteodermine may require proximity to the stratum superficiale (and possibly
268 even the adjacent epidermis; de Buffrénil et al., 2011). For now, however, the developmental
269 origins of osteodermine remain uncertain.
270 Mineralised collagen was found to be present throughout the ODs of *V. komodoensis*, but
271 whereas it stained green in Masson's trichrome in the outer region, the inner region stained red
272 indicating that the collagen is under tension within the core (Fig. 2D). *H. suspectum* ODs showed
273 the reverse condition, where more green staining occurred within the base and core of OD
274 compared to more red staining in the periphery and the complete lack of stain in the superficial

osteodermine regions (Fig. 1D). These differences in the distribution and tension of collagen within the osteoderms of the two species may affect the mechanical properties of the osteoderms under load and may be related to differences in the ecology of the two species.

Both *H. suspectum* and *V. komodoensis* demonstrate a comparable orthogonal arrangement of large collagen bundles within the dermis (Fig. 1 and 2, S.C., S.S.), and ODs from both species demonstrate a conspicuous basophilic line demarcating the limit of mineralisation, similar to that reported for *H. horridum* (Moss, 1969). Both species of *Heloderma*, but not *Varanus*, preserve the same herringbone organisation of collagen within the matrix of the tissue we identify as Sharpey-fibre bone (Fig. 1C, F, I; Moss 1969). S.F.B. in *Heloderma* exhibited multiple lacunae, and occasionally horizontal repeating darker lines of growth towards the basal layers of the OD (Fig. 1A, D, Asterisks), indicating mineralisation may occur radially from an initial central point, as reported in alligator ODs (Vickaryous & Hall, 2008). Both squamate and crocodilian ODs (de Buffrénil et al., 2010, 2015) have been hypothesised to originate via the formation of an initial nucleus of mineralisation, the developmental origins of which are currently uncertain, followed by remodeling to yield lamellar bone of osteoblastic origin. This could also be the path of development followed in helodermatid ODs, but further developmental studies are required to determine whether this is the case.

Unlike ODs in *Heloderma*, those of *V. komodoensis* did not demonstrate S.F.B. suggesting that the original arrangement of collagen fibres from the dermis of varanids were replaced and/or remodelled by newly laid fibres of parallel-fibred bone (Fig. 2E). Indeed, the mineralised collagen fibres of parallel-fibred bone were seen to be arranged in rings around a central core, with disruption to this lamellar orientation in the inner core where the collagen fibres became more woven and randomly orientated (Fig. 2D, F). When the parallel-fibred bone was compared to the mineralised mesh of orthogonal fibres observed in the S.F.B. region of *H. suspectum* (Fig. 1C, F, I) it was evident that *V. komodoensis* ODs exhibit different mineralised collagen structures (Fig. 2D, F). Lamellar bone was identified surrounding internal vasculature in *V. komodoensis* ODs (Fig. 2E), but the ODs of *V. komodoensis* were rarely seen to be vascularised in comparison

to *H. suspectum* ODs.

The results presented here provide evidence that the collagen structure of the dermis is not mirrored in the mineralised collagen observed within V*. komodoensis* ODs, as is the case in *H. suspectum* ODs*.* We observed a similarity between the radial concentric lines of arrested growth in the ODs of *V. komodoensis* (Fig. 2, Asterisks) and those of *H. suspectum* ODs (Fig. 1, Asterisks). These also resemble OD growth lines previously documented and used to estimate the age of specimens of *Varanus salvator* (Erickson et al., 2003). We showed that growth lines were also visible in osteodermine of *H. suspectum* ODs, as in *Tarentola mauritanica* ODs*,* where previous authors regarded them as an artefact of spheritic (globular) mineralisation (Levrat-Calviac and Zylberberg, 1986).

We observed L.B. in structures that resemble osteons and that display a "Maltese cross" formation when observed with polarised light microscopy and a "scalloped border" (Vickaryous & Hall, 2008) in histological staining. This suggests remodelling of the *H. suspectum* OD may occur. The presence of osteons as Haversian structures, in direct association and contact with S.F.B., suggests multiple mechanisms of formation in the ontogenesis of *H. suspectum* ODs – an initial mineralisation (not yet understood), then remodeling to form secondary Haversian structures (de Buffrénil et al., 2011), followed by the deposition of the osteodermine cap (Vickaryous et al., 2015).

Objective two: the histology of osteodermine and its distribution in *Heloderma suspectum*

Based on the below criteria, we identify the capping material on the ODs of *H. suspectum* as osteodermine. Histologically, osteodermine is characterised as a vitreous, highly mineralised and cell-poor tissue that lacks intrinsic collagen (de Buffrénil et al., 2011; Vickaryous et al., 2015). Osteodermine demonstrates weak staining for Alcian blue, indicating the presence of acid mucosubstances, but is not metachromatic with Toluidine blue; in addition, *H. suspectum* osteodermine is not birefringent under polarised light. As of the time of publication, osteodermine has now been identified in species of two distantly related genera: *Heloderma suspectum* (this study), *Heloderma horridum* (Moss, 1969), *Tarentola mauritanica* and *Tarentola*

annularis (Vickaryous et al., 2015), suggesting that the taxonomic distribution of this tissue remains to be recorded. Considering the homology of osteodermine across species, we were able to identify all the features previously used to define osteodermine in the sampled skin *H. suspectum*, and did not identify any additional, novel features in *H. suspectum* osteodermine. The ODs of *H. suspectum* are relatively large and are shown here as having very thick cap of osteodermine, thicker than in previously studied species (Vickaryous et al., 2015). *H. suspectum* is therefore a prime candidate species any for further research into this material.

Conclusions

The basal regions of *H. suspectum* ODs were found to be composed of Sharpey-fibre bone containing mineralised dermal collagen fibres, with lamellar bone sometimes found surrounding internal vasculature. Osteodermine was identified as the previously unnamed capping material (Moss, 1969). The ODs of *V. komodoensis* were found to be primarily composed of outer rings of parallel-fibred bone, with an inner core of woven bone, without evidence of osteodermine or Sharpey-fibre bone. Lamellar bone surrounding internal vasculature was observed once in *V. komodoensis* ODs but they are rarely vascularised in comparison to *H. suspectum.* The results presented here underscore the histological variability observed in ODs within lizards and suggest that the formation of ODs in *Varanus spp.* and *Heloderma spp.* may follow different developmental paths despite being relatively closely related.

Acknowledgements

The authors gratefully acknowledge funding from the Engineering and Physical Sciences Research Council (EP/1789616) and Human Frontier Science Program (RGP0039/2019). We would also like to thank the histology department at the UCL Institute of Neurology, the imaging suite at UCL Institute of Ophthalmology and the Zoological Society of London, London Zoo Pathology Department. The authors declare no conflict of interest.

Author Contributions

S.E., M.M. and S.B. conceived the project. S.E. provided the biological samples and aided in dissection. A.K. and A.B. performed experimental work. A.K. drafted the manuscript. A.K.,

M.V., A.B., A.O., M.M., S.B. and S.E edited and finalised the manuscript.

Data Availability Statement

All relevant data is presented in the results section and figures.

References

Boyde A, Felder A, Mills D (2019) New approach to increase information content in polarised light microscopy of skeletal and dental tissues. *Proc Microscience Microscopy Congress,* online abstract (https://www5.shocklogic.com/scripts/jmevent/programme.php?Client_Id=%27RMS%27&Project_Id=%27MMC2019%27&System_Id=1) accessed: 10/10/19

Calvi EN, Nahas FX, Barbosa MV, et al. (2012) An experimental model for the study of collagen fibers in skeletal muscle. *Acta Cir Bras* **27**, 681–686.

Campbell JA (1982) A new species of *Abronia* (Sauria, Anguidae) from the Sierra Juárez, Oaxaca, México. *Herpetologica* **38**, 355–361.

Cope ED (1869) [Protocol of the March 9, 1869 meeting]. *Proc Acad Nat Sci Philadelphia* **21,** 5

de Buffrénil V, Clarac F, Fau M, et al. (2015) Differentiation and growth of bone ornamentation in vertebrates: A comparative histological study among the Crocodylomorpha. *J Morphol* **276**, 425–445.

de Buffrénil V, Dauphin Y, Rage JC et al. (2011) An enamel-like tissue, osteodermine, on the osteoderms of a fossil anguid (Glyptosaurinae) lizard. *C R Palevol* **10**, 427–437.

de Buffrénil V, Sire JY, Rage JC (2010) The histological structure of glyptosaurine osteoderms (Squamata: Anguidae), and the problem of osteoderm development in squamates. *J Morphol* **271**, 729–737.

Dubansky BH, Dubansky BD (2018) Natural development of dermal ectopic bone in the American alligator (*Alligator mississippiensis*) resembles heterotopic ossification disorders in humans. *Anat Rec* **301**, 56–76.

Erickson, GM, de Ricqles A, de Buffrénil V, et al. (2003) Vermiform bones and the evolution of gigantism in *Megalania* : how a reptilian fox became a lion. J *Vertebr Paleontol* **23**, 966–970.

Flint MH, Merrilees MJ (1976) Relationship between the axial periodicity and staining of collagen by the Masson trichrome procedure. *Histochem J* **9**, 1–13.

Geoffroy Saint-Hilaire, E (1827). Description des Reptiles. In: *Description de l'Égypte ou recueil des observations et des recherches qui ont été faites en Égypte pendant l'expedition de l'Armée Française, publié par les ordres de sa Majesté l'Empere* (ed Savigny, MJCL). pp. 121–160 Paris, France: L'imprimerie impériale.

Haines RW, Mohuiddin A (1968) Sharpey-fibred bone. *J Anat* **103**, 527–538.

Hall BK (2015). *Bones and Cartilage: Developmental and Evolutionary Skeletal Biology.* London, UK: Elsevier.

Horner JR, Woodward HN, Bailleul AM (2016) Mineralised tissues in dinosaurs interpreted as having formed through metaplasia: a preliminary evaluation. *C R Palevol*, **15**, 183–203.

Kiernan J, Lillie R, Pizzolato P et al. (2010) Haematoxylin Eosin (H&E) Staining Protocols Online. https://www.protocolsonline.com/histology/dyes-and-stains/haematoxylin-eosin-he-staining/ accessed: 05/06/19.

Klymkowsky MW Hanken J (1991) Whole-mount staining of *Xenopus* and other vertebrates. In: *Xenopus laevis: Practical Uses in Cell and Molecular Biology. Methods in Cell Biology* 36 (eds Kay BK, Peng HB), pp. 419–428. London, UK: Elsevier.

Levrat-Calviac V, Zylberberg L (1986) The structure of the osteoderms in the gekko: *Tarentola mauritanica*. *Am J Anat* **176**, 437–46.

Linnaeus C (1766) *Systema naturae per regna tria natura*. 10th ed.,Tomus I: 1–4 Stockholm, Sweden: Laurentii Salvii.

Main RP, de Ricqlès A, Horner JR et al. (2005) The evolution and function of thyreophoran dinosaur scutes: implications for plate function in stegosaurs. *Paleobiology* **31**, 291–314.

Maisano JA, Laduc TJ, Bell CJ et al. (2019) The cephalic osteoderms of *Varanus komodoensis* as revealed by high-resolution X-ray computed tomography. *Anat Rec* **302**, 1675–1680.

Moss ML (1969) Comparative histology of dermal sclerifications in reptiles. *Cells Tissues Organs* **73**, 510–533.

Moss ML (1972) The vertebrate dermis and the integumental skeleton. *Integr Comp Biol* **12**, 27–34.

Ouwens PA (1912) On a large *Varanus* species from the island of Komodo. *Bull Jard Bo. Buitenzorg* **6**, 1–3.

Puchtler H, Waldrop FS (1979) On the mechanism of Verhoeff's elastica stain: a convenient stain for myelin sheaths. *Histochemistry* **62**, 233–247.

Stump CW, (1925) The histogenesis of bone. *J Anat* **59** (Pt 2) 136–154.

Vickaryous, MK, Meldrum G, Russell, AP (2015) Armored geckos: a histological investigation of osteoderm development in *Tarentola* (Phyllodactylidae) and *Gekko* (Gekkonidae) with comments on their regeneration and inferred function. *J Morphol* **276**, 1345–1357.

Vickaryous MK, Hall BK (2008) Development of the dermal skeleton in *Alligator mississippiensis* (Archosauria, Crocodylia) with comments on the homology of osteoderms. *J Morphol* **269**, 398–422.

Vickaryous MK, Sire JY (2009) The integumentary skeleton of tetrapods: origin, evolution, and development. *J Anat* **214**, 441–464.

Witten PE, Hall BK (2002) Differentiation and growth of kype skeletal tissues in anadromous male Atlantic Salmon (*Salmo salar*) Int. *J Dev Biol* **46**:719–730.

Zylberberg L, Castanet J (1985) New data on the structure and the growth of the osteoderms in the reptile *Anguis fragilis* (Anguidae, Squamata) *J Morphol* **186**, 327–342.

Figure Legends

Figure 1: Histological overview of *H. suspectum* OD in (A, D, G) parasagittal and (C, F, I) coronal sections stained with (A) Alcian blue, (B, C) H&E, (D-F) Masson's trichrome and (G-I) Verhoeff van Gieson. Also (B, E, H) coronal sections of unmineralised dermis for comparison. S.F.B. = Sharpey-fibre bone, L.B. = lamellar bone, OST. = osteodermine, S.C. = stratum compactum, S.S. = stratum superficiale, Asterisks = growth lines. Scale bars: All 200μm.

Figure 2: Histological overview of *V. komodoensis* OD stained with Alcian blue in (A) parasagittal and (B) coronal section, stained with Masson's trichrome in (C) parasagittal and (D) coronal section; and stained with Haematoxylin and Eosin in (E) parasagittal section and (F) coronal section. L.B. = lamellar bone, W.B. = woven bone, P.F.B. = parallel-fibred bone, S.C. = stratum compactum, S.S. = stratum superficiale, Asterisks = growth lines. Scale bars: (A) = 200μm, (B and C) = 100μm, (D) = 200μm, (E) = 100μm, (F) = 200μm.

Figure 3: (A) Parasagittal section of *H. suspectum* OD, (B) parasagittal section of *V. komodoensis* OD, (C) coronal section of *H. suspectum* OD, and (D) coronal section of *V. komodoensis* OD. (A-D) All stained with H&E and visualised with multi-rotation polarised light microscopy. S.F.B. = Sharpey-fibre bone, P.F.B. = parallel-fibred bone, W.B. = woven bone, S.C. = stratum compactum, white arrows = Sharpey's fibres. Scale bars: (A) = 50µm, (B) = 50µm, (C) = 250µm, (D) = 50µm.

Figure 4: (A and B) Parasagittal sections of *H. suspectum* OD stained with toluidine blue visualised with cross-polarised light microscopy. (C) *H. suspectum* OD, parasagittal section stained with Masson's Trichrome, visualised with multi-rotation polarised light microscopy and (D) same section as (C), visualised with light microscopy. S.F.B. = Sharpey-fibre bone, L.B. and red arrows = lamellar bone, OST. = osteodermine, S.C. = stratum compactum, S.S. = stratum superficiale, white arrows = Sharpey's fibres. Scale bars: All 100µm.

Supplementary Figure 1:
X-ray plate imaging of the dorsal skin of (A) *Heloderma suspectum* and (B) *Varanus komodoensis.* White indicates a denser material, black indicates a less dense material. The mineralised osteoderms thus appear white in comparison to the non-mineralised surrounding tissue. There are substantial differences in the overall shape and degree of tessellation between the two species. Scale bars: 5mm

Suggested Cover Image: An uncropped version of the image shown in Figure 3C. Polarised light micrograph of a coronal section of *H. suspectum* osteoderm and surrounding dermis. False colour composite created from six images taken with crossed linearly polarising filters at 15º rotation intervals, merged in the colour circle sequence Red, Yellow, Green, Cyan, Blue, Magenta. Colour shows the orientation within the section plane, with four repeat cycles in 360º. Brightness is proportional to the cosine of the strike angle with respect to section plane, being brightest in plane, and black when perpendicular to that plane, i.e., parallel to the optic axis. Dark central patch corresponds to the region that was mineralised. Width of field = 3.04mm

Table legends

Supplementary Table 1: A list of included histological stains, a description of their general characteristics and colour interpretation of the results.

Supplementary Material:

480

Histochemical stain	Utility	Colour results
H&E (Haematoxylin and eosin)	Shows general nuclear and cytoplasmic morphology.	Nuclei: Blue Cytoplasm, collagen: Pink Bone, osteoid: Pink-Purple
Masson's Trichrome	Shows collagen and keratin	Collagen: Green/Blue Nuclei: Black Muscle, cytoplasm, keratin: Red
E.V.G./V.V.G. (Elastic/Verhoeff Van Gieson)	Shows elastic fibres	Collagen: Red Elastic fibres: Black
Alcian Blue	Shows acid mucosubstances/ carboxylated glycosaminoglycans and acid mucins	Acid mucosubstances: Blue Nuclei: Red Cytoplasm: Pink
Toluidine Blue	Standard Light: Shows general morphology/ mineralisation of bone matrix	Acidic tissue compounds (incl. DNA, RNA): Blue
	Polarised light: Arrangement, orientation of collagen	Collagen: Birefringent blue/orange

Supplementary Table 1: A list of included histological stains, a description of their general characteristics and colour interpretation of the results.

481

482

483

484

485

486

487

488

489

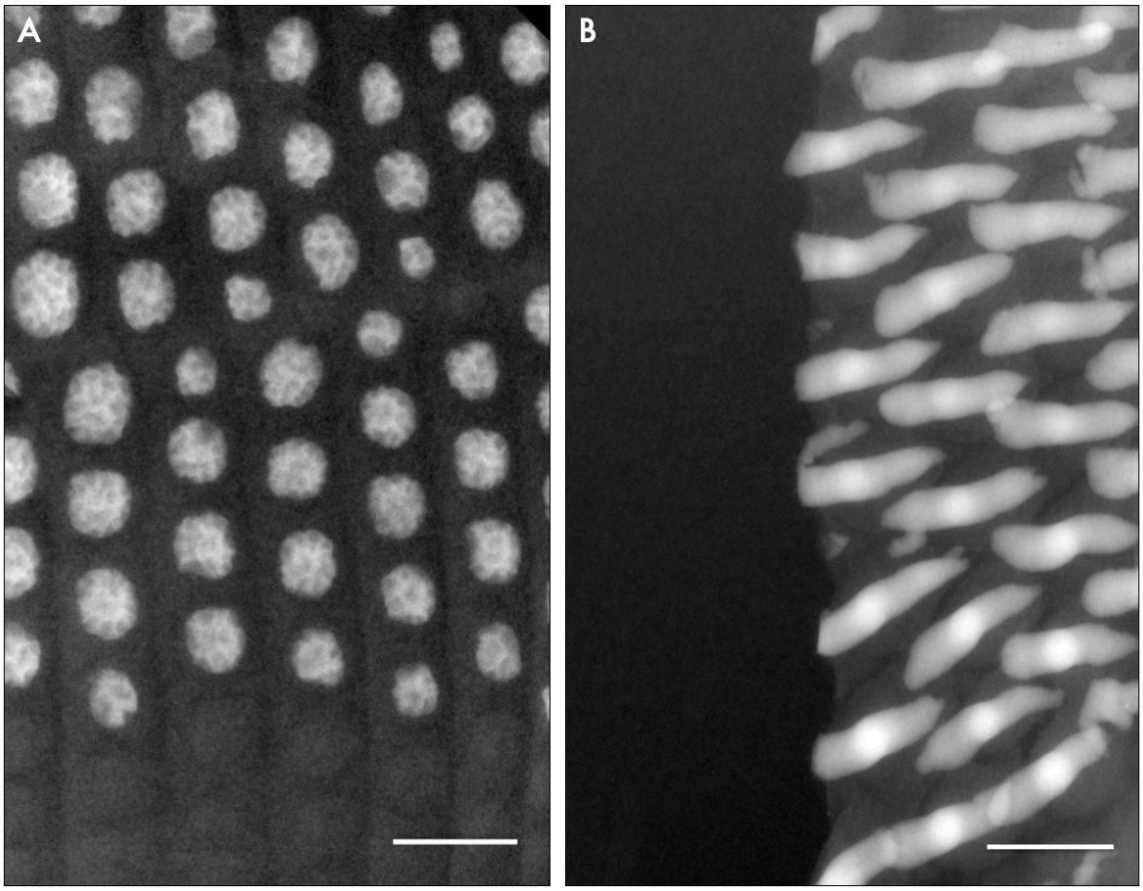

Supplementary Figure 1: X-ray plate imaging of the dorsal skin of (A) *Heloderma suspectum* and (B) *Varanus komodoensis.* White indicates a denser material, black indicates a less dense material. The mineralised osteoderms thus appear white in comparison to the non-mineralised surrounding tissue. There are substantial differences in the overall shape and degree of tessellation between the two species. Scale bars: 5mm

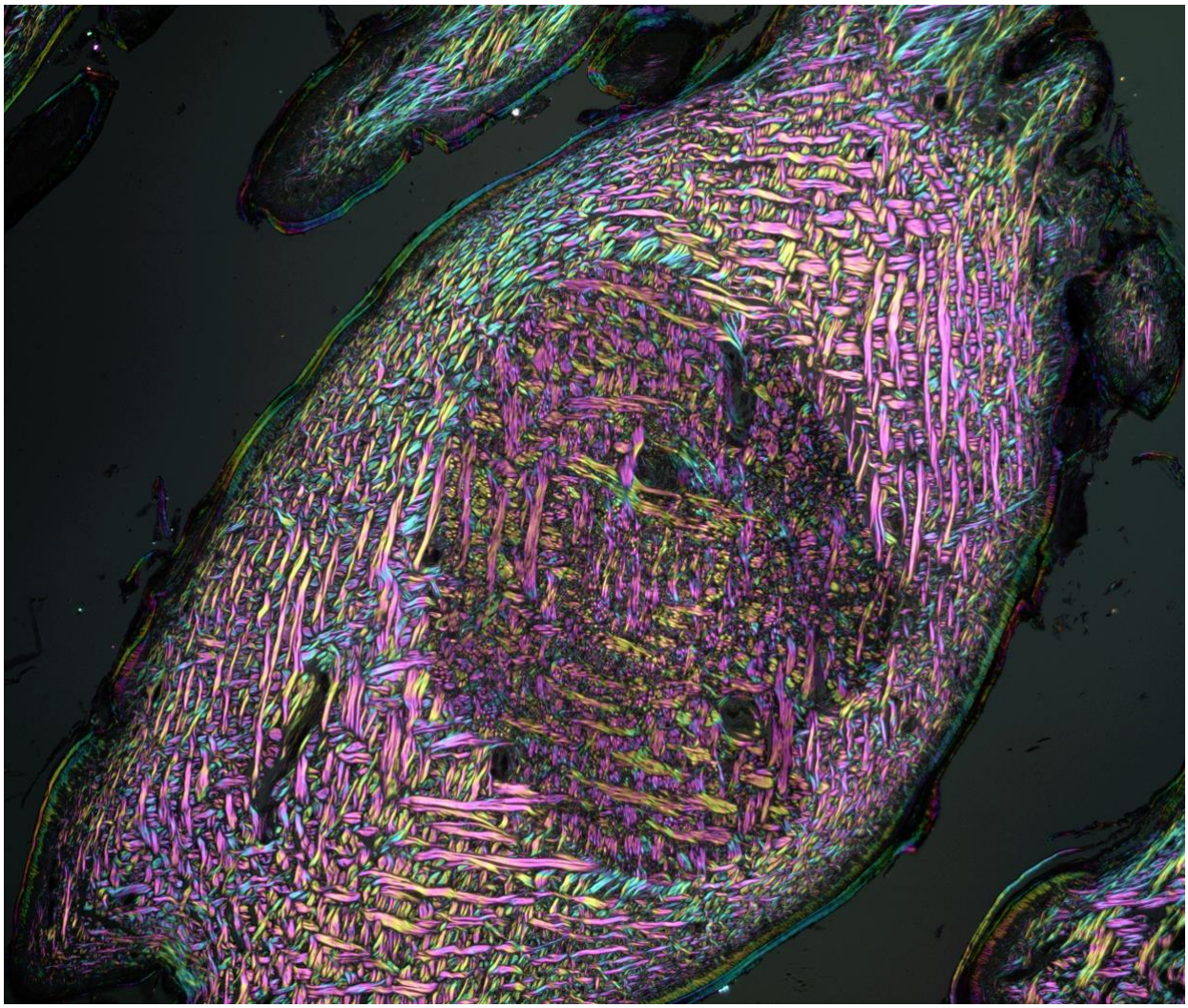

Suggested Cover Image: An uncropped version of the image shown in Figure 3C. Polarised light micrograph of a coronal section of *H. suspectum* osteoderm and surrounding dermis. False colour composite created from six images taken with crossed linearly polarising filters at 15º rotation intervals, merged in the colour circle sequence Red, Yellow, Green, Cyan, Blue, Magenta. Colour shows the orientation within the section plane, with four repeat cycles in 360º. Brightness is proportional to the cosine of the strike angle with respect to section plane, being brightest in plane, and black when perpendicular to that plane, i.e., parallel to the optic axis. Dark central patch corresponds to the region that was mineralised. Width of field = 3.04mm